Numer Algor (2019) 81:79–98
https://doi.org/10.1007/s11075-018-0536-9

ORIGINAL PAPER

Galerkin approach for estimating boundary data in Poisson equation on annular domain with application to heat transfer coefficient estimation in coiled tubes

Fermin S. V. Bazán[1] · **J. R. Quiroz**[1]

Received: 1 September 2017 / Accepted: 26 April 2018 / Published online: 5 May 2018

Abstract We investigate the problem of reconstructing internal Neumann data for a Poisson equation on annular domain from discrete measured data at the external boundary. By applying a Galerkin's collocation method to the direct problem, the reconstruction problem is formulated as a linear system and boundary data are determined through a singular value decomposition (SVD)-based scheme. The SVD of the coefficient matrix is explicitly determined, and thus regularization methods such as truncated singular value decomposition (TSVD) and Tikhonov regularization (TR) are readily implemented. Numerical examples using both synthetic and experimental data are presented to illustrate the efficiency of the method, including an application to the experimental estimation of heat transfer coefficients in coiled tubes; the regularization parameter for TSVD and TR is determined by the discrepancy principle.

Keywords Cauchy problem · Truncated SVD · Tikhonov regularization · Morozov's discrepancy principle

✉ Fermin S. V. Bazán
fermin.bazan@ufsc.br

J. R. Quiroz
jonathan17r@gmail.com

[1] Department of Mathematics, Federal University of Santa Catarina, Florianópolis SC, 88040-900, Brazil

1 Introduction

We consider a reconstruction problem for the Poisson equation on annular domain, specified by a 2D model in polar coordinates (r, θ) described as

$$\lambda_w \frac{1}{r}\frac{\partial}{\partial r}\left(r\frac{\partial T}{\partial r}\right) + \lambda_w \frac{1}{r^2}\frac{\partial^2 T}{\partial^2 \theta} + q_g = 0, \quad r_{\mathrm{I}} < r < r_{\mathrm{E}},\ 0 \le \theta \le 2\pi. \tag{1}$$

$$\lambda_w \frac{\partial T}{\partial r}(r_{\mathrm{E}}, \theta) = \alpha(T_{env} - T(r_{\mathrm{E}}, \theta)), \quad 0 \le \theta \le 2\pi \tag{2}$$

$$-\lambda_w \frac{\partial T}{\partial r}(r_{\mathrm{I}}, \theta) = Q(\theta), \quad 0 \le \theta \le 2\pi. \tag{3}$$

In heat conduction problems, the annular domain represents a cross-section of a duct with internal radius $0 < r_{\mathrm{I}}$ and external radius r_{E}, as shown in Fig. 1, λ_w denotes wall thermal conductivity, which is assumed constant, q_g is a source function, e.g., heat generated by Joule effect on the internal boundary, α is the reciprocal heat transfer resistance between the tube wall and the surrounding environment with temperature T_{env}, and Q is the heat flux distribution along the inner boundary. For future reference, the inner and outer boundaries of Ω are denoted by Γ_{I} and Γ_{E}, respectively. Our investigation is restricted to annular domains for two reasons. The first is that the annular domain is the shape of a cross-section of a pipe, as described above. The second is that, up to a conformal mapping, other domains such as doubly connected domains or square domains can be seen as annular domains [7, 19].

The boundary value problem (BVP) (1)–(3) is referred to as the forward or direct problem. The inverse problem consists of recovering the Neumann data Q from measured point-wise temperature data at the external boundary Γ_{E}: $\widetilde{T}_j = T(r_{\mathrm{E}}, \theta_j) + \epsilon_j$, $j = 0, \ldots, N$, where ϵ_j denotes random noise. Measurements like these can be

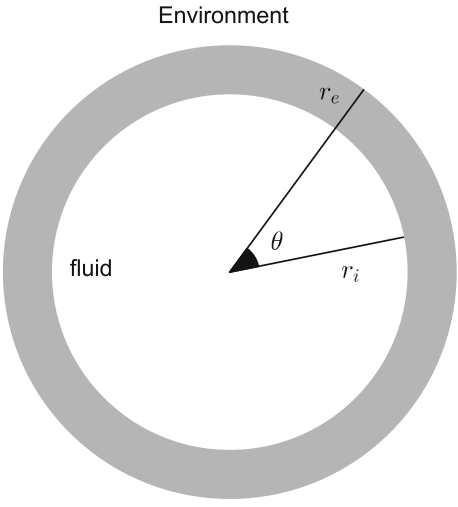

Fig. 1 Tube cross-section

obtained in several ways, e.g., using a infrared camera [8, 13]. This inverse problem arises in applications such as food processing, corrosion detection, non-nuclear power production, air-conditioning systems, and power electronics [7–9, 13, 24, 26, 29]. Unfortunately, inverse boundary value problems are generally ill-posed [6, 14] and therefore small perturbations in data may generate arbitrarily large perturbations in the numerical solutions, calling for the use of regularization methods.

Several algorithms have been proposed to overcome the ill-posed nature of inverse boundary value problems for elliptic equations. These include a Backus-Gilbert reconstruction algorithm for Laplace equation [18], numerical methods based on complex analysis tools for the Laplace equation on annular domain [19, 22], self-regularization methods [10], use of Model functions for heat flux reconstruction in pool boiling [17], and numerical algorithms that estimate Neumann data as preliminary step for reconstructing Robin data or heat transfer coefficients [1, 2, 8, 9, 12, 13, 15]. Related contributions are found in several places; for example, an spectral method for a Cauchy problem associated with the Laplace equation can be found in [7]. Mesh-less radial point interpolation methods are employed in [27, 28]. An inverse boundary element method (BEM) for determining the heat transfer coefficients on solid surfaces of arbitrary shape is described in [23].

A common feature of most of the methods mentioned above is the discretization of the direct problem in order to establish a linear map that relates the desired data to the measured data. In this work, we also follow this line; however, as we will see later, our approach is different since the dimension of the discretized problem is dictated by the number of samples and the reconstruction arises from the singular value decomposition (SVD) of a linear transformation. A differential feature of the proposed approach is that such SVD is obtained at no additional cost and as a consequence of the chosen discretization process. The rest of the paper is organized as follows. In Section 2, we construct approximate solutions to the direct problem by means of a Galerkin collocation method and derive preliminary results. In Section 3, supposing noise-free data, we describe a finite singular value expansion for Q, including regularization methods for the noisy case. Regularization is achieved by means of the TSVD method and Tikhonov regularization. The regularization parameter is determined by the Morozov's discrepancy principle [20]. In Section 4, we report numerical results that illustrate the efficiency of the reconstruction method using both synthetic and experimental data. The paper ends with concluding remarks in Section 5.

2 Forward problem: Galerkin collocation approach

The reconstruction method to be described in the next section lies in the observation that the solution to (1)–(3) can be expressed as

$$T = V + u, \tag{4}$$

where V and u solve, respectively, suitable auxiliary boundary value problems. There are several ways to express the solution T as in (4); see, e.g, [10, 13].

Here we construct T so that V solves the auxiliary homogeneous boundary value problem

$$\frac{\partial}{\partial r}\left(r\frac{\partial V}{\partial r}\right)+\frac{1}{r}\frac{\partial^2 V}{\partial\theta^2}=0,\quad r_{\mathrm{I}}<r<r_{\mathrm{E}},\ 0\le\theta\le 2\pi. \tag{5}$$

$$\lambda_w\frac{\partial V}{\partial r}(r_{\mathrm{E}},\theta)+\alpha V(r_{\mathrm{E}},\theta)=0,\quad 0\le\theta\le 2\pi \tag{6}$$

$$-\lambda_w\frac{\partial V}{\partial r}(r_{\mathrm{I}},\theta)=Q(\theta),\quad 0\le\theta\le 2\pi. \tag{7}$$

and u solves the auxiliary non-homogeneous boundary value problem

$$\mathrm{r}\frac{\partial}{\partial \mathrm{r}}\left(\mathrm{r}\frac{\partial u}{\partial \mathrm{r}}\right)+\frac{\partial^2 u}{\partial\theta^2}+q_g=0,\quad \mathrm{r}_{\mathrm{I}}<\mathrm{r}<\mathrm{r}_{\mathrm{E}},\ 0\le\theta\le 2\pi \tag{8}$$

$$\lambda_w\frac{\partial u}{\partial \mathrm{r}}(\mathrm{r}_{\mathrm{E}},\theta)=\alpha(T_{env}-u(\mathrm{r}_{\mathrm{E}},\theta)=0,\quad 0\le\theta\le 2\pi \tag{9}$$

$$-\lambda_w\frac{\partial u}{\partial \mathrm{r}}(\mathrm{r}_{\mathrm{I}},\theta)=0,\quad 0\le\theta\le 2\pi. \tag{10}$$

Since our interest is to construct approximate solutions to (5)–(7) through a Galerkin collocation method, motivated by physical considerations, we will assume that V and V_θ are 2π-periodic, that is

$$V(r,0)=V(r,2\pi),\quad \frac{\partial V}{\partial\theta}(r,0)=\frac{\partial V}{\partial\theta}(r,2\pi)\quad r_{\mathrm{I}}<r<r_{\mathrm{E}}, \tag{11}$$

and consider the Fourier basis

$$R_0(\theta)=1,\quad R_k(\theta)=\cos(k\theta),\ S_k(\theta)=\sin(k\theta),\ k=1,\ldots,$$

It is well known that family $\{R_0,R_1,S_1,\ldots,\}$ form an orthogonal basis for the Hilbert space $L^2(0,2\pi)$ with standard inner product [21]

$$\langle u,v\rangle=\int_0^{2\pi}u(\theta)v(\theta)d\theta \tag{12}$$

With the Fourier basis at hand, we follow [11, 25] and look for approximated solutions of the form

$$V_M(r,\theta)=v_0R_0(\theta)+\sum_{k=1}^{M}v_k(r)R_k(\theta)+w_k(r)S_k(\theta) \tag{13}$$

where the coefficients $\{v_k,w_k\}$ are to be determined. To this end, we replace V_M into (5), multiply the resulting equality by R_k, S_k, and then integrate in $(0,2\pi)$. This leads to

$$\int_0^{2\pi}\left[\frac{\partial}{\partial r}\left(r\frac{\partial V_M}{\partial r}\right)+\frac{1}{r}\frac{\partial^2 V_M}{\partial\theta^2}\right]R_k(\theta)d\theta=0,\qquad k=0,\ldots,M. \tag{14}$$

$$\int_0^{2\pi}\left[\frac{\partial}{\partial r}\left(r\frac{\partial V_M}{\partial r}\right)+\frac{1}{r}\frac{\partial^2 V_M}{\partial\theta^2}\right]S_k(\theta)d\theta=0,\qquad k=1,\ldots,M. \tag{15}$$

Since the functions $\{R_k,\ S_k\}_{k=0}^{M}$ are orthogonal, (14)–(15) reduce to

$$r^2 v_k''(r) + r v_k'(r) - k^2 v_k(r) = 0, \quad r_{\mathrm{I}} < r < r_{\mathrm{E}} \tag{16}$$

$$r^2 w_k''(r) + r w_k'(r) - k^2 w_k(r) = 0, \quad r_{\mathrm{I}} < r < r_{\mathrm{E}} \tag{17}$$

and the boundary condition (6) yields

$$\lambda_w v_k'(r_{\mathrm{E}}) + \alpha v_k(r_{\mathrm{E}}) = 0, \qquad \lambda_w w_k'(r_{\mathrm{E}}) + \alpha w_k(r_{\mathrm{E}}) = 0. \tag{18}$$

Since in the numerical treatment of the inverse problem we will deal with pointwise data, we enforce $V_M(r,\theta)$ to satisfy the boundary condition (7) by replacing the Neumann data Q by its trigonometric interpolant at uniformly spaced points. Given $Q_j \doteq Q(\theta_j)\ j = 0,\dots,N-1$, where θ_j are uniformly spaced points in $[0, 2\pi]$, $\theta_j = j2\pi/N,\ j = 0,\dots,N-1$, it is well known that there exists a unique trigonometric polynomial $\widehat{Q}_N(\theta)$ satisfying the interpolation conditions $\widehat{Q}_N(\theta_j) = Q_j,\ j = 0,\dots,N-1$. Its coefficients depend on N being odd or even and can be determined explicitly. For instance, for odd N and n such that $N-1 = 2n$, the interpolating polynomial is given by

$$\widehat{Q}_N(\theta) = \frac{a_0}{2} + \sum_{k=1}^{n} a_k R_k(\theta) + b_k S_k(\theta). \tag{19}$$

with coefficients

$$\begin{aligned} a_k &= \frac{2}{N}\sum_{j=0}^{N-1} Q_j R_k(\theta_j), \quad k = 0,\dots,n, \\ b_k &= \frac{2}{N}\sum_{j=0}^{N-1} Q_j S_k(\theta_j), \quad k = 1,\dots,n. \end{aligned} \tag{20}$$

Similar results can be deduced for even N. For future reference, we notice that the expressions in (20) come from the fact that the vectors $\mathbf{r}_k, \mathbf{s}_k \in \mathbb{R}^N$ defined by

$$\begin{aligned} \mathbf{r}_k &= [R_k(\theta_0),\dots,R_k(\theta_{N-1})]^T,\ k = 0,\dots,n, \\ \mathbf{s}_k &= [S_k(\theta_0),\dots,S_k(\theta_{N-1})]^T,\ k = 1,\dots,n \end{aligned} \tag{21}$$

are orthogonal and fulfill [25]

$$\begin{aligned} \mathbf{r}_i^T \mathbf{r}_j &= \begin{cases} 0 \ \text{ if } \ i \neq j \\ N \ \text{ if } \ i = j = 0, \\ N/2 \ \text{ if } \ i = j = 1,\dots,n. \end{cases} \\ \mathbf{s}_i^T \mathbf{s}_j &= \begin{cases} 0 \ \text{ if } \ i \neq j \\ N/2, \ \ i = j = 1,\dots,n. \end{cases} \end{aligned} \tag{22}$$

Thus, for V_N to satisfy the boundary condition (7) with $\widehat{Q}_N$ instead of Q, it is required that

$$-\lambda_w \sum_{i=0}^{M} v_k'(r_{\mathrm{I}}) R_k(\theta) + w_k'(r_{\mathrm{I}}) S_k(\theta) = \widehat{Q}_N(\theta) \tag{23}$$

and the L^2-orthogonality of $\{R_0, R_1, S_1, \ldots, R_M, S_M\}$, $M > N$, gives

$$\begin{cases} -\lambda_w v_k'(r_{\mathrm{I}}) = a_k/d_k, & -\lambda_w w_k'(r_{\mathrm{I}}) = b_k; \quad k = 0, \ldots, N \\ -\lambda_w v_k'(r_{\mathrm{I}}) = 0, & -\lambda_w w_k'(r_{\mathrm{I}}) = 0; \quad k = N+1, \ldots, M \end{cases} \tag{24}$$

where $d_k = 2$ if $k = 0$ or $d_k = 1$ if $k = 1, \ldots, M$. This last result together with (16) show that, to determine the coefficients v_k, w_k, we must solve the boundary value problems;

$$\begin{cases} r^2 v_k''(r) + r v_k'(r) - k^2 v_k(r) = 0, & r_{\mathrm{I}} < r < r_{\mathrm{E}} \\ \lambda_w v_k'(r_{\mathrm{E}}) + \alpha v_k(r_{\mathrm{E}}) = 0 \\ -\lambda_w v_k'(r_{\mathrm{I}}) = a_k/d_k, \end{cases} \tag{25}$$

$$\begin{cases} r^2 w_k''(r) + r w_k'(r) - k^2 w_k(r) = 0 & r_{\mathrm{I}} < r < r_{\mathrm{E}} \\ \lambda_w w_k'(r_{\mathrm{E}}) + \alpha w_k(r_{\mathrm{E}}) = 0 \\ -\lambda_w w_k'(r_{\mathrm{I}}) = b_k. \end{cases} \tag{26}$$

Standard procedures show that for $k = 0$ the solution of (25) is

$$v_0(r) = \frac{a_0}{2}\left(\frac{r_{\mathrm{I}}}{\lambda_w}\ln\frac{r_{\mathrm{E}}}{r} + \frac{r_{\mathrm{I}}}{\alpha r_{\mathrm{E}}}\right). \tag{27}$$

For $k = 1, \ldots, N$, we seek solutions of the form

$$v_k(r) = c_{1,k} r^k + c_{2,k} r^{-k} \tag{28}$$

where the coefficients $c_{1,k}$ and $c_{2,k}$ are to be determined by using the boundary conditions in (25). Doing so it follows that the coefficients $c_{1,k}, c_{2,k}$ satisfy the linear system

$$\begin{cases} c_{1,k} r_{\mathrm{E}}^{2k}(\lambda_w k + \alpha r_{\mathrm{E}}) + c_{2,k}(\alpha r_{\mathrm{E}} - \lambda_w k) = 0 \\ c_{1,k} r_{\mathrm{I}}^{2k} - c_{2,k} = -a_k r_{\mathrm{I}}^{k+1}/\lambda_w k \end{cases} \tag{29}$$

whose solutions are

$$\begin{aligned} c_{1,k} &= \frac{a_k r_{\mathrm{I}}^{k+1}(\lambda_w k - \alpha r_{\mathrm{E}})}{\lambda_w k\left(\lambda_w k(r_{\mathrm{E}}^{2k} - r_{\mathrm{I}}^{2k}) + \alpha r_{\mathrm{E}}(r_{\mathrm{E}}^{2k} + r_{\mathrm{I}}^{2k})\right)} \\ c_{2,k} &= \frac{a_k r_{\mathrm{E}}^{2k} r_{\mathrm{I}}^{k+1}(\alpha r_{\mathrm{E}} + \lambda_w k)}{\lambda_w k\left(\lambda_w k(r_{\mathrm{E}}^{2k} - r_{\mathrm{I}}^{2k}) + \alpha r_{\mathrm{E}}(r_{\mathrm{E}}^{2k} + r_{\mathrm{I}}^{2k})\right)}. \end{aligned} \tag{30}$$

Letting $\rho = r_{\mathrm{I}}/r_{\mathrm{E}}$, after rearrangement (28) results in,

$$v_k(r) = a_k \eta_k(r), \quad k = 0, \ldots \tag{31}$$

where

$$\begin{aligned} \eta_0(r) &= \left(\frac{r_{\mathrm{I}}}{\lambda_w}\ln\frac{r_{\mathrm{E}}}{r} + \frac{r_{\mathrm{I}}}{\alpha r_{\mathrm{E}}}\right), \\ \eta_k(r) &= \frac{(1 - \frac{\alpha r_{\mathrm{E}}}{\lambda_w k})\rho^k\left(\frac{r}{r_{\mathrm{E}}}\right)^k + (1 + \frac{\alpha r_{\mathrm{E}}}{\lambda_w k})\left(\frac{r_{\mathrm{I}}}{r}\right)^k}{\left[\lambda_w k(1 - \rho^{2k}) + \alpha r_{\mathrm{E}}(1 + \rho^{2k})\right]} r_{\mathrm{I}}, \quad k = 1, \ldots \end{aligned} \tag{32}$$

and a similar procedure shows that

$$w_k(r) = b_k \eta_k(r), \quad k = 1, \ldots \tag{33}$$

Notice that for $k = N+1, \ldots, M$ in (24), we obtain $v_k(r) = 0$ and $w_k(r) = 0$. Hence, it is enough considering V_N instead of V_M.

Proposition 2.1 *Given values Q_j at uniformly spaced points in $[0, 2\pi]$ as described above, the approximate solution of (1)–(3) obtained by the Galerkin collocation method is of the form*

$$V_N(r,\theta) = v_0(r)R_0(\theta) + \sum_{k=1}^{N} v_k(r)R_k(\theta) + w_k(r)S_k(\theta) \tag{34}$$

with coefficients given in (27), (28), and (33). Moreover, provided $Q \in L^2[0, 2\pi]$, we have

$$|v_k(r)|,\ |w_k(r)| \to 0 \ \ as \ \ k \to \infty \ \forall r \in (r_I, r_E]. \tag{35}$$

Proof The statement regarding V_N is true by construction. To prove the remaining part, we let $\rho = r_{\mathrm{I}}/r_{\mathrm{E}}$ and notice that

$$|c_{1,k}r^k| \le \frac{|a_k|r_{\mathrm{I}}|(\lambda_w k - \alpha r_{\mathrm{E}})|}{\lambda_w k(\lambda_w k + \alpha r_{\mathrm{E}})(1-\rho^{2k})}\rho^k \left(\frac{r}{r_{\mathrm{E}}}\right)^k, \tag{36}$$

and

$$|c_{2,k}r^{-k}| \le \frac{|a_k|r_{\mathrm{I}}}{\lambda_w k(1-\rho^{2k})}\left(\frac{r_{\mathrm{I}}}{r}\right)^k. \tag{37}$$

The inequalities show that if $|a_k|$ is bounded then $v_k(r)$ goes to zero exponentially as k grows $\forall\ r \in (r_{\mathrm{I}}, r_{\mathrm{E}}]$. For $w_k(r)$ we obtain a similar result; this completes the proof. □

An important consequence of the analysis above is that the coefficients $v_k(r)$ and $w_k(r)$ will become negligible for small or moderate k provided the coefficients a_k are bounded as occurs, e.g., for $Q \in L^2(0, 2\pi)$. Indeed, in such a case, the interpolation polynomial coefficients behave at least like $\mathcal{O}(1/k)$, which is sufficient to ensure that both $|c_{1,k}r^k|$ and $|c_{2,k}r^k|$ will become negligible for small k because of the bounds (36)–(37). To illustrate this observation, we consider data Q_j for a heat flux defined by $Q(\theta) = -3250 - 1265\exp(\cos\theta)$ with $N = 257$. Physical parameters are taken from [8], where the source function q_g is constant, $q_g = 4.8 \times 10^6$, $r_{\mathrm{I}} = 0.014$, $r_{\mathrm{E}} = 0.015$, $\lambda_w = 15$, $\alpha = 5$, and $T_e = 294.2$. The size of both $|a_k|$ and $|v_k(r)|$ as a function of k, displayed in Fig. 2, shows that both quantities become negligible for k near 15; hence, approximately $k = 15$ terms in (34) are sufficient to capture the most important features of the solution V. An approximate solution obtained with 15 terms, $V_{15}(r,\theta)$, is displayed in Fig. 3.

Taking into account both the way as V_N is constructed and approximation results regarding the interpolation error $Q - \widehat{Q}_N$ [11, 25], the following result is a consequence of the Lax-Milgram Theorem.

Proposition 2.2 *Let $V_N(r,\theta)$ as in the previous proposition. As $N \to \infty$, $V_N(r,\theta)$ converges to $V \in L^2(0, 2\pi)$ in the L^2-sense and V is a weak solution of (5)–(7).*

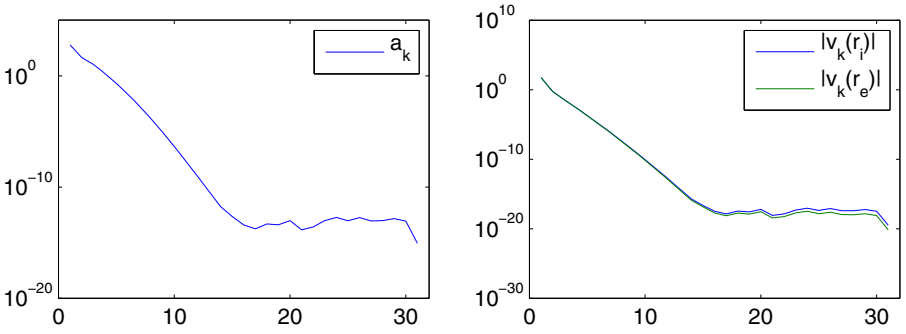

Fig. 2 Coefficients $|a_k|$ and $|v_k(r)|$ for $k = 0, \ldots, 30$

We observe that to complete the solution T, we still have to solve the auxiliary problem (8)–(10), which, for a general source function, must be done numerically. Indeed, this can be done by the Galerkin method as well or by any other method. We observe also that in the case where the source function is constant, such auxiliary problem reduces to

$$\begin{aligned} &\tfrac{1}{r}(ru'(r))' + q_g = 0, \quad r_{\mathrm{I}} < r < r_{\mathrm{E}} \\ &\lambda_w u'(r_{\mathrm{E}}) = \alpha(T_{env} - u(r_{\mathrm{E}})) \\ &u'(r_{\mathrm{I}}) = 0 \end{aligned}$$

whose solution is the radial function

$$u(r) = -\frac{q_g}{4\lambda_w}(r^2 - r_{\mathrm{E}}^2) + \frac{q_g}{2\lambda_w} r_{\mathrm{I}}^2 \ln(r/r_{\mathrm{E}}) + T_{env} + \frac{q_g}{2\alpha r_{\mathrm{E}}}(r_{\mathrm{E}}^2 - r_{\mathrm{I}}^2). \tag{38}$$

Industrial applications involving constant source functions are often met in inverse heat transfer problems [1, 8, 12, 13].

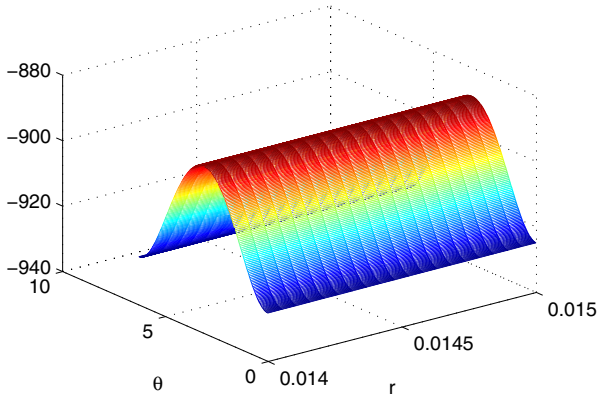

Fig. 3 Approximate solution $V_{15}(r, \theta)$

3 The inverse problem

Perhaps the most important consequence of the theoretical results described in the previous section is that we can construct approximate solutions for (1)–(3) of excellent quality by simply taking N sufficiently large. In this section, we will concentrate on a method for estimating heat flux data based on such solutions. Let the approximate solution for (1)–(3) be expressed as $T_N(r,\theta) \doteq V_N(r,\theta) + u(r,\theta)$, where $V_N(r,\theta)$ is determined by using the Galerkin collocation method as described before, that is

$$T_N(r,\theta) = \frac{a_0}{2}\eta_0(r)R_0(\theta) + \sum_{k=1}^{n} \eta_k(r)\left(a_k R_k(\theta) + b_k S_k(\theta)\right) + u(r,\theta)$$

with $\eta_k(r)$ defined in (32). Assume that $u(r,\theta)$ is available or easy to calculate and that we are given data values of $T_N(r_{\mathrm{E}},\theta)$ at the Fourier collocation points $\theta_j,\ j = 0,\ldots,N-1$. We are going to show that with the "measured data" $\mathsf{G}_j = T_N(r_{\mathrm{E}},\theta_j) - u(r_{\mathrm{E}},\theta_j),\ j = 0,\ldots,N-1$ at hand we will be able to:

i) Compute temperature values $T_N(r,\theta_j)$ for all $r \in [r_{\mathrm{I}}, r_{\mathrm{E}}]$;
ii) Establish a linear map of the form

$$\mathsf{A_N Q} = \mathsf{G}$$

where $A_N \in \mathbb{R}^{N\times N}$ and Q, G are vectors of point-wise values of Q and measured data values respectively.

In fact, rewrite $V_N(r_{\mathrm{E}},\theta)$ as

$$V_N(r_{\mathrm{E}},\theta) = \frac{a_0}{2}\check{\eta}_0 R_0(\theta) + \sum_{k=0}^{n} \check{\eta}_k\left(a_k R_k(\theta) + b_k S_k(\theta)\right) \tag{39}$$

where $\check{\eta}_k = \eta(r_{\mathrm{E}})$,

$$\check{\eta}_0 = \frac{\rho}{\alpha}, \quad \check{\eta}_k = \frac{2\rho^k}{\lambda_w k\left(1-\rho^{2k}\right) + \alpha r_{\mathrm{E}}\left(1+\rho^{2k}\right)} r_{\mathrm{I}},\ k = 1,\ldots,n, \tag{40}$$

and then notice that the data vector G can be described as

$$\mathsf{G} = \begin{bmatrix} V_N(r_{\mathrm{E}},\theta_0) \\ \vdots \\ V_N(r_{\mathrm{E}},\theta_{N-1}) \end{bmatrix} = \mathsf{E_N D_N C} \tag{41}$$

where $\mathsf{E_N} = [\frac{\mathbf{r}_0}{2}, \mathbf{r}_1, \mathbf{s}_1, \ldots, \mathbf{r}_n, \mathbf{s}_n]$, with $\mathbf{r}_k, \mathbf{s}_k$ as in (21), $\mathsf{D_N} = \mathrm{diag}\left(\check{\eta}_0, \check{\eta}_1, \check{\eta}_1, \ldots, \check{\eta}_n, \check{\eta}_n\right)$ and $\mathsf{C} = [a_0, a_1, b_1, \ldots, a_n, b_n]$. Recognizing that $\mathsf{E_N}$ has orthogonal columns due to (22) and that $\mathsf{E_N}^T\mathsf{E_N} = \mathsf{B} = \mathrm{diag}(N/4, N/2, \ldots, N/2) \in \mathbb{R}^{N\times N}$, it follows that the interpolation coefficients satisfy

$$\mathsf{C} = \mathsf{D_N}^{-1}\mathsf{B}^{-1}\mathsf{E_N}^T\mathsf{G}. \tag{42}$$

Let $\mathsf{G}^{(r)}$ denote the vector with entries $\mathsf{G}_j^{(r)} = T_N(r,\theta_j) - u(r,\theta_j)$, $j = 0,\ldots,N-1$. It is obvious that, like (41), we have

$$\mathsf{G}^{(r)} = \mathsf{E_N}\mathsf{D_N^{(r)}}\mathsf{C}, \tag{43}$$

where $\mathsf{D_N}^{(r)} = \mathrm{diag}\,(\eta_0(r), \eta_1(r), \eta_1(r), \ldots, \eta_n(r), \eta_n(r))$. Hence, by virtue of (42), we have

$$\mathsf{G}^{(r)} = \mathsf{E_N}\mathsf{D_N^{(r)}}\mathsf{D_N}^{-1}\mathsf{B}^{-1}\mathsf{E_N}^T\mathsf{G} \tag{44}$$

and this shows that item i) is achieved. Item ii) appears as a consequence of the proof of the Proposition below.

Proposition 3.1 *With the notation and definitions in (39)–(41), assume that we are given noiseless data $T_N(r_E,\theta_j)$ where θ_j, $j = 0,\ldots,N-1$, denote, as before, the Fourier collocation points. Then, the vector Q of point-wise values Q_j of Q can be expressed as*

$$\mathsf{Q} = \mathsf{F_N}\mathsf{D_N^{-1}}\mathsf{F_N}^T\mathsf{G} = \sum_{k=1}^{N}\frac{\mathsf{f}_k^T\mathsf{G}}{\sigma_k}\mathsf{f}_k, \tag{45}$$

where $\mathsf{F_N} = \mathsf{E_N}\sqrt{\mathsf{B}^{-1}}$, $\mathsf{f_k}$ denotes the k-th columns of $\mathsf{F_N}$ and $\sigma_1 = \check{\eta}_0$, $\sigma_{2i} = \sigma_{2i+1} = \check{\eta}_i$, $i = 1,\ldots,n$, with $\check{\eta}_i$ defined in (40). Moreover, the vector T of point-wise values of $T(r,\theta_j)$ can be described as

$$\mathsf{T} = \sum_{k=1}^{N}\frac{\eta_k(r)\mathsf{f}_k^T\mathsf{G}}{\sigma_k}\mathsf{f}_k + \mathsf{u}, \tag{46}$$

where u denotes the vector of point-wise values of $u(r,\theta_j)$.

Proof Since (20) implies $\mathsf{C} = \mathsf{B}^{-1}\mathsf{E_N}^T\mathsf{Q}$, substitution of C into (41) shows that Q solves a linear system of the form

$$\mathsf{A_N}\mathsf{Q} = \mathsf{G}, \qquad \mathsf{A_N} = \mathsf{E_N}\mathsf{D_N}\mathsf{B}^{-1}\mathsf{E_N^T}. \tag{47}$$

Recognizing that $\mathsf{F_N} = \mathsf{E_N}\sqrt{\mathsf{B}^{-1}}$ is an orthogonal matrix, it follows that $\mathsf{A_N}$ has a singular value decomposition (SVD) expressed as

$$\mathsf{A_N} = \mathsf{F_N}\mathsf{D_N}\mathsf{F_N}^T, \tag{48}$$

and this implies (45). The expression in (46) follows immediately from (44). □

Despite the relevance of having found an explicit representation for the vector of heat flux values, we emphasize that the main hypothesis of the proposition is not entirely realistic, since what is to be measured are values of T not of T_N. For this reason, for the reconstruction of Q, we will assume that:

a) the function $u(r_E,\theta)$ is simple to evaluate or calculated to high precision,
b) the approximation error $|T(r_E,\theta) - T_N(r_E,\theta)|$ is negligible to such an extent that we can substitute $T_j = T(r_E,\theta_j)$ for $T_N(r_E,\theta_j)$ without any significant loss.

It is worth mentioning that assumption a) is automatically satisfied in inverse heat transfer problems where the source function represents uniform heating generated

by Joule effect. For other cases cases, the solution $u(r_{\mathrm{E}}, \theta)$ must be computed by a highly accurate method. As for assumption b), recall that the coefficients v_k, w_k become negligible for small k (see Prop. 2.1 and Fig. 2). Thus, assumption b) is valid when N is large enough, which is not a restriction due to the current availability of modern data acquisition equipment.

However, in practice, we only have perturbed data $T_\delta(\theta_j) = T(r_{\mathrm{E}}, \theta_j) + \epsilon_j, \ \ j = 0, \ldots, N-1$, which, for inversion purposes, generate input data G_δ such that

$$\|\mathsf{G} - \mathsf{G}_\delta\|_2 \leq \delta. \tag{49}$$

So the challenge is to determine meaningful approximations to Q by solving the linear system (47) with G_δ instead of G. The major difficulty here is that, as the matrix $\mathsf{A_N}$ is severely ill-conditioned due to the fast decrease of its singular values (see Fig. 4), the computed solution $\mathsf{Q}_\delta = \mathsf{A_N}^{-1}\mathsf{G}_\delta$ will be contaminated by noise in such a way that it will have no practical value.

We illustrate this by considering the reconstruction problem using data generated by the heat flux $Q(\theta)$ described in the previous section. Exact and perturbed data used in this illustration as well as the vector Q and Q_δ are all displayed in Fig. 5. A way to see this more precisely is by using the SVD of A_N. Indeed, if we let $\mathsf{G}_\delta = \mathsf{G} + \varepsilon$ where ε stands for a vector of inaccuracies, then the computed solution can be expressed as

$$\mathsf{Q}_\delta = \sum_{k=1}^{N} \frac{\mathsf{f}_k^{\mathsf{T}}\mathsf{G}_\delta}{\sigma_k}\mathsf{f}_k = \mathsf{Q} + \sum_{k=1}^{N} \frac{\mathsf{f}_k^{\mathsf{T}}\epsilon}{\sigma_k}\mathsf{f}_k, \tag{50}$$

where the sum on the right equality stands for the perturbation error. As the singular values rapidly decrease to zero, the above expression shows that the perturbation error will dominate the final result because in practice, there is no way to prevent

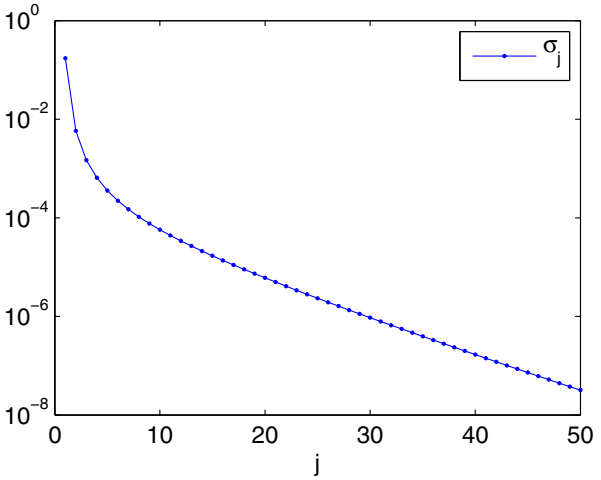

Fig. 4 Behavior of σ_j

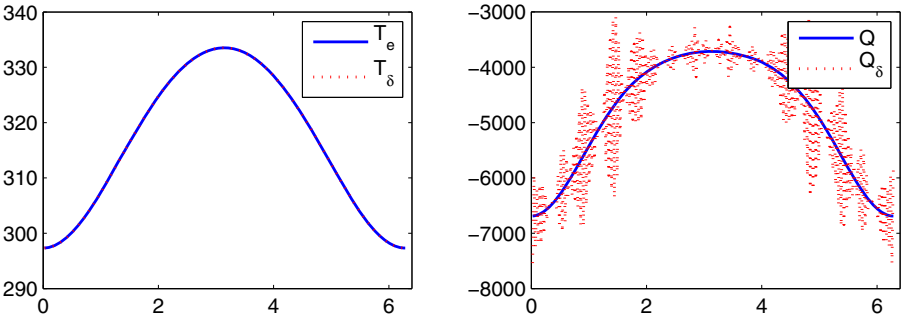

Fig. 5 Left: exact and perturbed temperature data: $T(r_{\mathrm{E}}, \theta_j)$, $\widetilde{T}(r_{\mathrm{E}}, \theta_j) = T(r_{\mathrm{E}}, \theta_j) + \epsilon_j$, $j = 0, \ldots 256$ (i.e., $N = 257$), for noise vector ϵ with standard deviation 7.8954×10^{-6}. Right: exact heat flux and its naive reconstruction

σ_k from being much less than $|\mathsf{f}_k^{\mathsf{T}}\varepsilon|$ for some k; this explains the ill-posed nature of the reconstruction problem addressed in this work. Thus, regularization methods are required in order to construct approximations that resemble the exact solution Q. □

3.1 Regularized solutions

As already seen in (50), the main problem with Q_δ is that noise components can be greatly amplified because of the division by small singular values; in this event, the computed estimate Q_δ can differ enormously from Q. To filter out the contribution of noise to the computed solution, two regularization methods will be used in this work, namely, truncated SVD (TSVD) and Tikhonov regularization.

3.1.1 TSVD

Since the reconstructed heat flux from noisy data is dominated by inaccuracies, based on the SVD of matrix A_N (48), the TSVD method determines regularized solutions by truncating the sum (50) to k terms, see, e.g., [16], giving rise to regularized solutions defined as

$$\mathsf{Q}_\delta^{(\mathsf{k})} = \sum_{j=1}^{\mathsf{k}} \frac{\mathsf{f}_j^{\mathsf{T}}\mathsf{G}_\delta}{\sigma_j}\mathsf{f}_j.$$

The point here is that if k is poorly chosen, the solution $\mathsf{Q}_\delta^{(k)}$ either captures not enough information about the problem or the noise in the data dominates the approximate solution. The challenge in connection with TSVD is thus how to choose a proper truncation parameter. In this work, the truncation parameter is determined according to the discrepancy principle (DP) of Morozov [20]; i.e., for the truncation parameter, we choose the first index k such that

$$\|\mathsf{A}_\mathsf{N}\mathsf{Q}_\delta^{(\mathsf{k})} - \mathsf{G}_\delta\|_2 \leq \tau\delta, \ \ \tau \gtrsim 1. \tag{51}$$

3.1.2 Tikhonov method

Tikhonov regularization (TR) manages ill-conditioned systems by solving nearby least-squares problems. In our context, TR determines approximate solutions by solving the penalized least-squares problem

$$\mathsf{Q}_{\lambda,\delta} = \underset{\mathsf{Q}\in\mathbb{R}^N}{\operatorname{argmin}} \mathsf{J}_\lambda(\mathsf{Q}), \quad \mathsf{J}_\lambda(\mathsf{Q}) = \|\mathsf{A}_\mathsf{N}\mathsf{Q} - \mathsf{G}_\delta\|_2^2 + \lambda^2\|\mathsf{Q}\|_2^2,$$

where $\lambda > 0$ is the regularization parameter. The functional $\mathsf{J}_\lambda(\mathsf{Q})$ represents a trade-off between two optimization processes: the fidelity of the fit and second the smoothness or the stability of the solution. Thus, for the regularized solution $\mathsf{Q}_{\lambda,\delta}$ to be meaningful the regularization parameter must balance both processes. In other words, the choice of a good regularization parameter requires a good balance between the size of the residual norm and the size of the solution norm [16]. Regarding the practical aspects, based on the SVD of A_N, it is immediate to see that the regularized solution can be expressed as

$$\mathsf{Q}_{\lambda,\delta} = \sum_{j=1}^{\mathsf{N}} \frac{\sigma_j \mathsf{f}_j^\mathsf{T}\mathsf{G}_\delta}{(\lambda^2 + \sigma_j^2)}\mathsf{f}_j.$$

In this work, the regularization parameter will be chosen according DP; i.e., for the regularization parameter, we choose the only root of the non-linear equation [20]

$$\|\mathsf{A}_\mathsf{N}\mathsf{Q}_{\lambda,\delta} - \mathsf{G}_\delta\|_2 = \tau\delta, \quad \tau \gtrsim 1. \tag{52}$$

Based on the SVD of A_N again, it is straightforward to see that the squared residual norm

$$R(\lambda) := \|\mathsf{A}_\mathsf{N}\mathsf{Q}_{\lambda,\delta} - \mathsf{G}_\delta\|_2^2.$$

is an increasing function of the regularization parameterλ, so the non-linear equation (52) can be readily solved; see, e.g., [3, 16].

We end the section with the observation that error bounds associated to regularized solutions obtained by TSVD and TR with DP as parameter choice rule are well established in literature and are therefore not included here.

4 Numerical results

We shall now illustrate the effectiveness of the proposed method by describing reconstruction results using both synthetic and experimental data.

4.1 Reconstructions using synthetic data

Case 1: Constant source function

We consider a test problem with temperature data generated by means of the Galerkin approach, as described in Section 2, with heat flux defined by

$$Q(\theta) = -3250 - 1265\exp(\cos\theta).$$

Physical parameters are taken from [8] and reproduced here for convenience:

$$\alpha = 5,\ \lambda_w = 15,\ q_g = 4.8 \times 10^6,\ T_{env} = 294.2,\ T_b = 295.2,\ r_{\mathrm{E}} = 0.015. \quad (53)$$

For the inverse problem, we consider $N = 127$ temperature values $\widetilde{T}_j = T(r_{\mathrm{E}}, \theta_j) + \epsilon_j$, where ϵ_j are zero mean random numbers scaled such that the corresponding data vectors satisfy

$$\mathsf{T}_\delta = \mathsf{T} + \mathrm{NL}\|\mathsf{T}\|\epsilon, \quad \|\epsilon\| = 1,$$

where NL stands for relative noise level. Hence, the data vector for inversion is

$$\mathsf{G}_\delta = \mathsf{T}_\delta - u(r_{\mathrm{E}})\mathbf{1}$$

where $\mathbf{1}$ denotes the vector of all ones and u is determined according to (38), and thus

$$\delta = \|\widetilde{\mathsf{T}} - \mathsf{T}\| = \|\mathsf{G}_\delta - \mathsf{G}\| = \mathrm{NL}\|\mathsf{T}\|.$$

To quantify the effectiveness of the new method at distinct noise levels, we define the relative estimation error for Q as

$$\mathrm{EQ} = \|\mathsf{Q}_{\mathrm{estimated}} - \mathsf{Q}_{\mathrm{exact}}\|_2 / \|\mathsf{Q}_{\mathrm{exact}}\|_2,$$

For the test problem under consideration, we ran 100 instances with different data vectors sharing the same noise level. We report average relative errors corresponding to five noise levels $\mathrm{NL} = 10^{-6}, 10^{-5}, \ldots, 10^{-2}$ and five distinct inner radii $r_{\mathrm{I}} = 0.010, 0.011, 0.012, 0.013, 0.014$. All calculations were carried out using Matlab with the error norm δ as input data. Recall that the error norm δ is required for the implementation of TSVD and TR based on the discrepancy principle as regularization parameter choice rule.

Numerical results obtained in the experiment are displayed in Fig. 6. Two conclusions can be drawn from the results. First, TSVD and TR produce results of comparable quality, and second, the quality of the reconstructions tends to deteriorate as the inner radius decreases. While the first observation confirms common experience widely described in literature, the second one expresses the fact that the problem becomes more sensitive to noise as the inner radius decreases. To reinforce this last observation, the condition number of A_{N} as a function of the inner radius is displayed in Table 1.

Results obtained in the first run for two noise levels are displayed in Fig. 7.

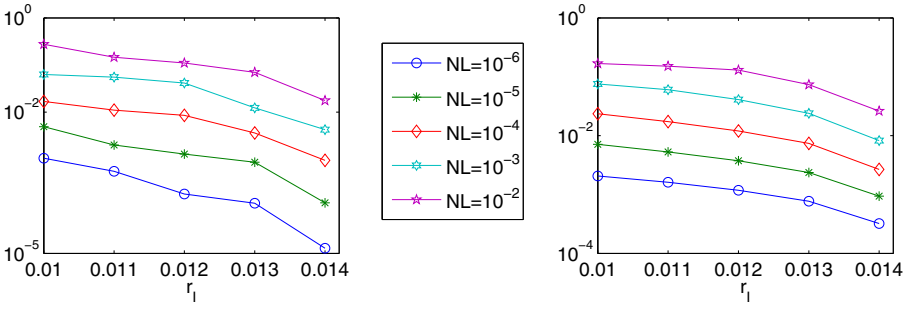

Fig. 6 Average relative errors EQ for several noise levels and several inner radii. Left: TSVD-based results. Right: Tikhonov regularization-based results

Table 1 Condition numbers of matrix A_N

r_I	0.010	0.011	0.012	0.013	0.014
$\kappa(A_N)$	4.4351×10^{26}	2.2317×10^{21}	3.2486×10^{16}	1.1538×10^{12}	8.7603×10^{7}

Case 2: Variable source function

We consider a test problem with source function $q_g(r,\theta)$ chosen in such a way that the exact solution to the forward problem (1)–(3) and the heat flux are defined by

$$T(r,\theta)=\frac{Q(\theta)}{\alpha}\exp\left[-\frac{\alpha}{\lambda_w}(r-r_I)\right],\quad Q(\theta)=\frac{0.5\alpha\left[3+\cos^2(0.5\theta)\right]}{\alpha+0.5\alpha\left[3+\cos^2(0.5\theta)\right]}(T_b-T_{env}).$$

In this numerical experiment, the "physical" parameters are chosen as

$$r_I=0.4,\ r_E=0.9,\ T_b=55,\ T_{env}=10,\ \alpha=8,\ \lambda_w=5.$$

As the source function depends on both variables r and θ, to determine the "exact" data set for inversion, $G(r_E,\theta_j)=T(r_E,\theta_j)-u(r_E,\theta_j),\ j=0,\ldots,N$, the solution $u(r,\theta_j)$ to the auxiliary problem (8)–(10) is obtained numerically through the highly accurate Chebyshev pseudospectral method, as made in [1]. In this case, the solution is computed on a grid with $p=30$ points in the radial direction and $N=128$ points in the θ direction. With exact data set at hand, we proceed in the same way as before

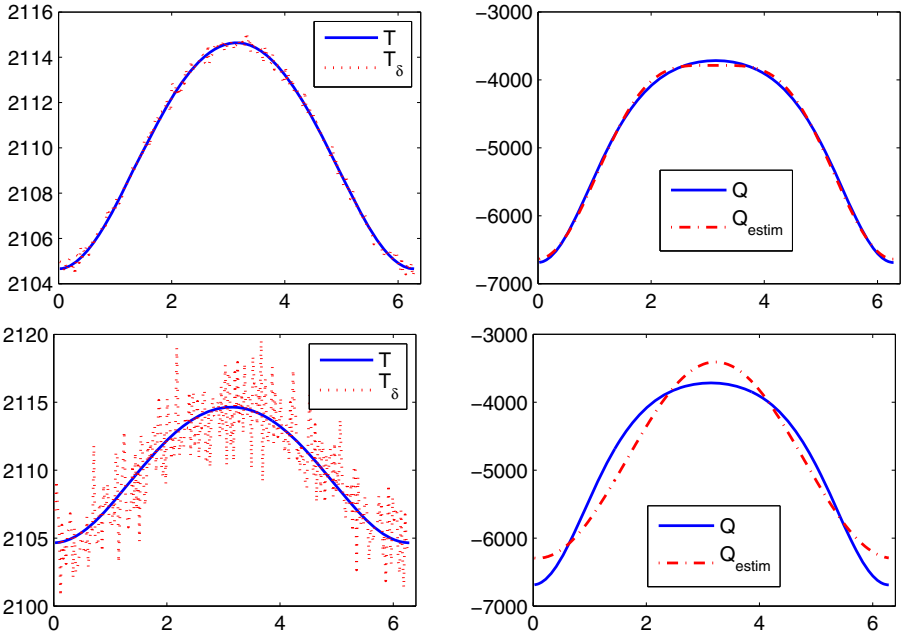

Fig. 7 Temperature data and estimated heat flux obtained with TSVD method. The results correspond to $r_I=0.013$, NL $=10^{-4}$ (top), and NL $=10^{-3}$ (bottom)

in order to simulate data for inversion with several noise levels. Average results of 100 realizations for noise levels NL $= 10^{-5}, \ldots, 10^{-2}$ produced reconstruction errors EQ ranging from 2.13×10^{-5} to 5.73×10^{-3}. Exact and noisy data, as well as exact and recovered heat flux (first run), are displayed in Fig. 8. As in Case 1, TSVD and TR produced results of comparable quality; that is why results obtained with TR are not shown here.

4.2 Reconstruction of heat transfer coefficient in coiled tubes: reconstruction using experimental data

In this section, we give an application of the method proposed in this work to the estimation of the heat transfer coefficient in coiled tubes from experimental temperature data at the external boundary acquired by Bozzoli et al. [8]. The estimation procedure relies on the fact that if the heat flux Q is available, then the heat transfer coefficient can be determined as [1, 8, 12, 13, 24]

$$h(\theta) = \frac{Q(\theta)}{T_b - T(r_{\mathrm{I}}, \theta)}, \quad T_b \neq T(r_{\mathrm{I}}, \theta),$$

where T_b denotes the bulk-fluid temperature on the test section (annular region) and $T(r_{\mathrm{I}}, \theta)$ denotes the temperature at the inner boundary associated to the heat flux Q.

The data consist of 276 point-wise equally spaced temperature values acquired by a infrared camera on the exterior test section wall surface of a stainless steel coiled tube under the prescribed condition of uniform heating generated by Joule effect in the tube wall (i.e., the source function g_g is constant). With the exception that in this experimental investigation the inner and external radii are $r_{\mathrm{I}} = 0.008$ mm and $r_{\mathrm{E}} = 0.009$ mm, the remaining physical parameters are the same as in (53). Experimental data acquired by the infrared camera are displayed in Fig. 9. The data clearly reveal that the temperature distribution exhibits a significant variation along the circumference, and the temperature gradient is almost negligible along the axis of the tube. This observation confirms that adopting a 2-D numerical model for this type of problem is appropriate. The experimental investigation was carried out in laminar

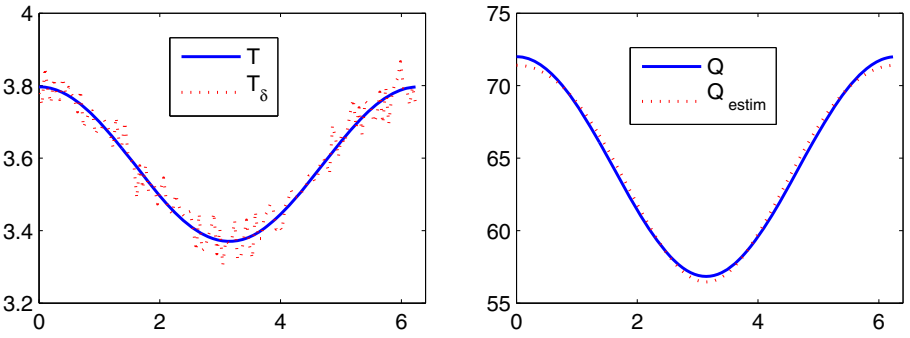

Fig. 8 Temperature data and estimated heat flux obtained with TSVD method. The results correspond to NL $= 10^{-2}$

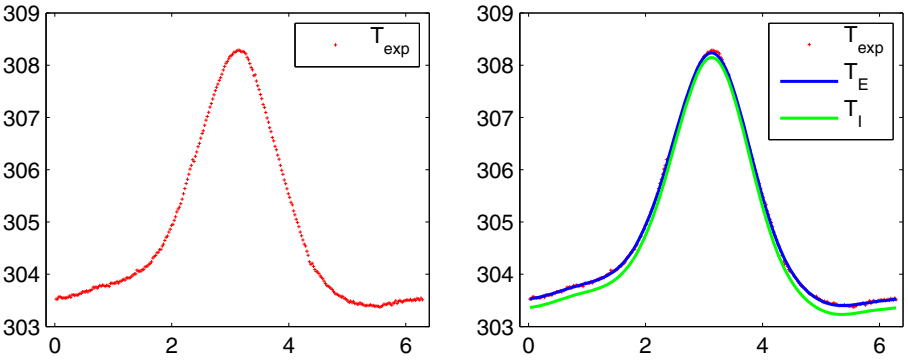

Fig. 9 Experimental data and recovered data

regime by using Ethylene Glycol as a working fluid. For further details about the experimental procedure, the reader is referred to Bozzoli [8].

Turning to the estimation procedure, as we know, for the implementation of the discrepancy principle, the error norm δ has to be estimated. In this experimental investigation, such estimation was made by measuring the surface temperature distribution while maintaining the coil wall under isothermal conditions [8]. Numerically, the truncation parameter determined by the discrepancy principle for TSVD was $k = 11$ and the regularization parameter for TR was $\lambda = 1.2093 \times 10^{-4}$. With the heat flux at hand, the heat transfer coefficient is estimated as

$$[\mathsf{h}_{\text{estim}}]_j = \frac{[\mathsf{Q}_{\text{estim}}]_j}{T_b - [\mathsf{T}_{\text{I}}]_j}, \quad j = 1, \ldots, N$$

where T_{I} denotes the temperature at the inner tube wall calculated according to Proposition 3.1 as

$$\mathsf{T}_{\text{I}} = \sum_{j=1}^{k} \frac{\eta_j(r_{\text{I}})\mathsf{f}_j^T \mathsf{G}}{\sigma_j}\mathsf{f}_j + u(r_{\text{I}}),$$

with k determined by the discrepancy principle.

Both reconstructions, heat flux and heat transfer coefficient, are displayed in Fig. 10. As we can see, the results agree well with those obtained in [8] where the forward problem is solved by the finite element method and the heat flux is determined by solving a regularized linear least-squares problem with a sensitivity matrix as a discrete forward operator. In that case, Tikhonov regularization is coupled with a fixed-point method to determine the regularization parameter [4, 5].

Filtered temperature data computed by truncating the sum given in (46) to k terms are compared to the experimental data in Fig. 9 (right). The results show that both reconstructed temperature distributions fit well the experimental data.

We conclude the section with reconstruction results of asymmetrical heat flux and asymmetrical heat transfer coefficient from experimental data provided by M. J. Colaço [13]. In this case, the data set consists of 201 temperature values acquired by

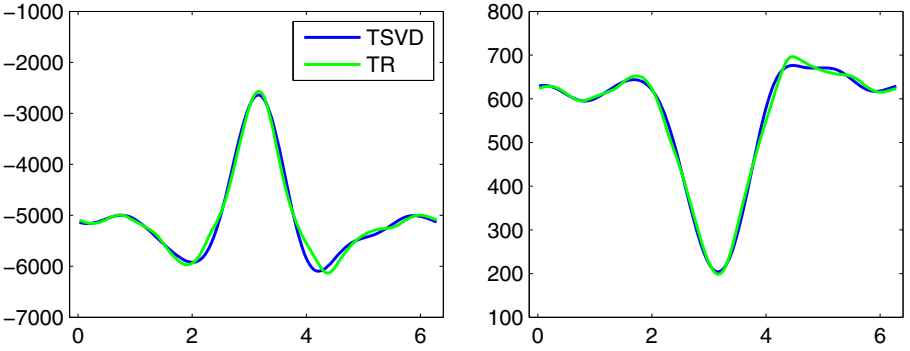

Fig. 10 Estimated heat flux Q and estimated heat transfer coefficient h from experimental measurements

an infrared camera, under the same experimental conditions as described above, and with physical parameters

$$q_g = 4.78 \times 10^6,\ T_b = 21.57,\ T_{env} = 23.85,\ \alpha = 5,\ \lambda_w = 15.$$

Experimental data for this numerical example are displayed in Fig. 11 (left). Filtered temperature data are displayed in Fig. 11 (right). As before, the results show that both reconstructed temperature distributions fit well the experimental data. Note that the filtered temperature values at the outer and inner boundaries are very similar. The reason of this is that the tube thickness is very small: $r_{\mathrm{E}} - r_{\mathrm{I}} = 0.001$. Finally, reconstructed heat flux and reconstructed heat transfer coefficient are depicted in Fig. 12. The results show that the method is also suitable for these types of non-symmetric functions. The reconstructed heat transfer coefficient obtained by our method looks very similar to that obtained in [13, Figure 6].

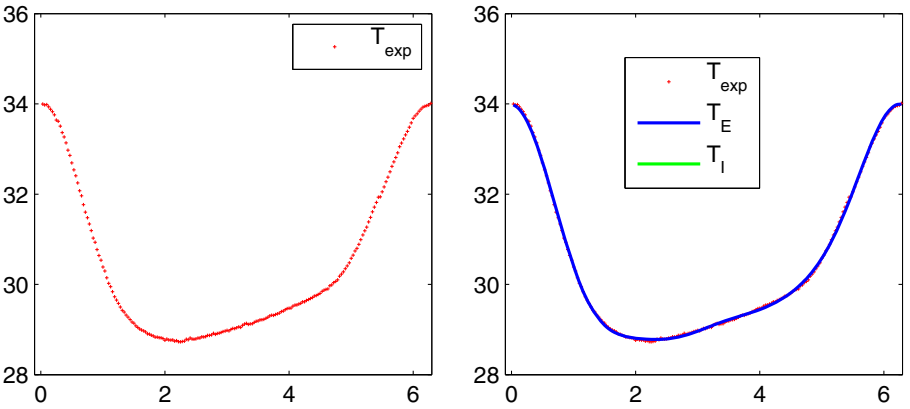

Fig. 11 Experimental data and recovered data: asymmetric case

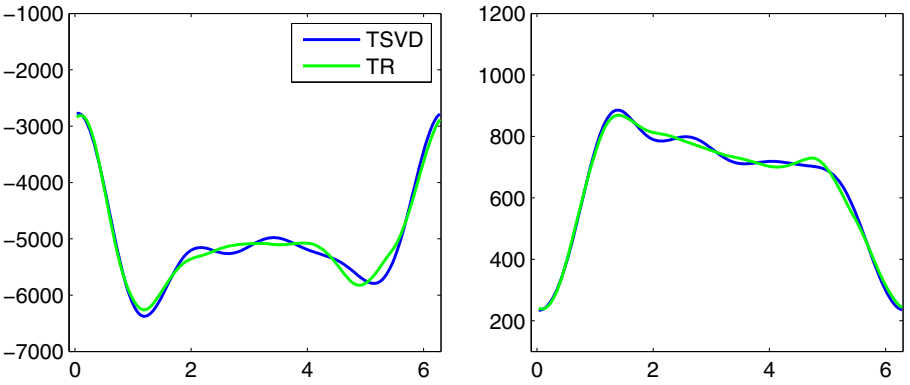

Fig. 12 Estimated heat flux Q (left) and estimated heat transfer coefficient h (right) from experimental measurements: asymmetric case

5 Conclusion

In this work, we investigated the problem of reconstructing boundary data for a Poisson equation on annular domain using discrete data. As the main result, we derive a method for reconstructing Neumann data at the internal (hence inaccessible) boundary using discrete measured data at the external (accessible) boundary. The method addresses the problem via Galerkin's method in such a way that point-wise boundary data are connected with measured data through a severely ill-conditioned linear system with boundary data as unknown. Our main contribution is an explicit description of the SVD of the coefficient matrix and hence an explicit SVD expansion of point-wise boundary data for the noisy-free case. Moreover, for the case of noisy data, two regularization methods are discussed and implemented, namely TSVD and Tikhonov regularization. The method is extremely simple to implement and computationally inexpensive since the reconstruction spends only a few standard inner products of low dimensional vectors. Several numerical results are included to illustrate the effectiveness of the proposed method. Finally, as an application, we estimate the heat transfer coefficient in coiled tubes from experimental data reported in [8, 13].

Funding information The work of both authors was supported by CNPq, Brazil, grant 308523/2017-2.

References

1. Bazán, F.S.V., Bedin, L., Bozzoli, F.: Numerical estimation of convective heat transfer coefficient through linearization. Int. J. Heat Mass Transf. **2**, 1230–1244 (2016)
2. Bazán, F.S.V., Bedin, L.: Identification of heat transfer coefficient through linearization: explicit solution and approximation. Inverse Probl. 25 **33**, 124006 (2017)
3. Viloche Bazán, F.S.: Simple and efficient determination of the Tikhonov regularization parameter chosen by the generalized discrepancy principle for discrete ill-posed problems. J. Sci. Comput. **63**(1), 163–184 (2015)
4. Bazán, F.S.V.: Fixed-point iterations in determining the Tikhonov regularization parameter. Inverse Probl. **24**, 1–15 (2008)

5. Bazán, F.S.V., Francisco, J.B.: An improved fixed-point algorithm for determining a Tikhonov regularization parameter. Inverse Probl. **25**, 045007 (2009)
6. Beck, J.V., Blackwell, B. .Jr., Clair, Ch.R.: Inverse Heat Conduction - Ill-Posed Problems. Wiley, New York (1985)
7. Bernston, F., Eldén, L.: Numerical solution of a Cauchy problem for the Laplace equation. Inverse Probl. **17**(4), 839–853 (2001)
8. Bozzoli, F., Cattani, L., Rainieri, S., Bazán, F.S.V., Borges, L.S.: Estimation of the local heat-transfer coefficient in the laminar flow regime in coiled tubes by Tikhonov regularisation method. Int. J. Heat Mass Transf. **72**, 352–361 (2014)
9. Cao, H., Pereverzev, S.V., Sincich, E.: Natural linearization for corrosion identification. J. Phys. Conf. Ser. **135**, 012027 (2008)
10. Cao, H., Pereverzev, S.V.: Balancing principle for the regularization of elliptic Cauchy problems. Inverse Prob. **23**, 1943–1961 (2007)
11. Canuto, C., Hussaini, M.Y., Quarteroni, A.A., Zang, T.A.: Spectral Methods in Fluid Dynamics. Springer-Verlag, Berlin (1988)
12. Chen, H.T., Wu, X.Y.: Estimation of heat transfer coefficient in two-dimensional inverse heat conduction problems. Numer. Heat Transfer Part B **50**, 375–394 (2006)
13. Colaço, M.J., Alves, C.J., Bozzoli, F.: The reciprocity function approach applied to the non-intrusive estimation of spatially varying internal heat transfer coefficients in ducts: numerical and experimental results. Int. J. Heat Mass Transfer. **90**, 1221–1231 (2015)
14. Engel, H.W., Hanke, M., Neubauer, A.: Regularization of Inverse Problems. Kluwer Academic Publishers (2000)
15. Fasino, D., Inglese, G.: An inverse Robin problem for Laplace's equation: theoretical results and numerical methods. Inverse Probl., 41–48 (1999)
16. Hansen, P.C.: Rank-Deficient and Discrete Ill-Posed Problems. SIAM, Philadelphia (1988)
17. Heng, Y., Mhamdi, A., Lu, Sh., Pereverzev, S.: Model functions in the modified L-curve method-case study: the heat flux reconstruction in pool boiling. Inverse Probl. **26**(5) (2010)
18. Hong, Y.G., Wei, T.: Backus-Gilbert algorithm for the Cauchy problem of the Laplace equation. Inverse Probl. **17**, 261–271 (2001)
19. Jaoua, M., Leblond, J., Mahjoub, M., Partington, J.R.: Robust numerical algorithms based on analytic approximation for the solution of inverse problems in annular domains. IMA. J. Appl. Math. **74**, 481–506 (2009)
20. Morozov, V.A.: Regularization Methods for Solving Incorrectly Posed Problems. Springer-Verlag, New York (1984)
21. Kirsch, A.: An Introduction to the Mathematical Theory of Inverse Problems. Springer-Verlag, New York (2011). Applied Mathematical Sciences 120
22. Leblond, J., Mahjoub, M., Partington, J.R.: Analytic extensions and Cauchy-type inverse problems on annular domains: stability results. J. Inv. Ill-Posed Probl. **14**(2), 189–204 (2006)
23. Martin, T.J., Dulikravich, G.S.: Inverse determination of steady heat convection coefficient distributions. J. Heat Transfer **120**, 328–334 (1998)
24. Naphon, P., Wongwises, S.: A review of flow and heat transfer characteristics in curved tubes. Renew. Sustain. Energy Rev. **10**, 463–490 (2006)
25. Peiret, R.: Spectral Methods for Incompressible Viscous Flow. Springer, Heildeberg (2002)
26. Pakdaman, M.F., Akhavan-Behabadi, M.A., Razi, P.: An experimental investigation on thermophysical properties and overall performance of MWCNT/heat transfer oil nanofluid flow inside vertical helically coiled tubes. Exper. Thermal Fluid Sci. **40**, 103111 (2012)
27. Shivanian, E., Jafarabadi, A.: Inverse Cauchy problem of annulus domains in the framework of spectral meshless radial point interpolation. Engineering with Computers. https://doi.org/10.1007/s00366-016-0482-x
28. Shirzadi, A., Takhtabnoos, F.: A local meshless method for Cauchy problem of elliptic PDEs in annulus domains. J. Inverse Probl. Sci. Eng. **24**, 729–743 (2016)
29. Tajani, C., Abouchabaka, J., Abdoun, O.: Data recovering problem using a new KMF algorithm for annular domain. Amer. J. Comp. Math. **2**, 88–94 (2012)